

Probabilistic Object Maps for Long-Term Robot Localization

Amanda Adkins

Taijing Chen

Joydeep Biswas

Abstract—Robots deployed in settings such as warehouses and parking lots must cope with frequent and substantial changes when localizing in their environments. While many previous localization and mapping algorithms have explored methods of identifying and focusing on long-term features to handle change in such environments, we propose a different approach – can a robot understand the distribution of movable objects and relate it to observations of such objects to reason about global localization? In this paper, we present probabilistic object maps (POMs), which represent the distributions of movable objects using pose-likelihood sample pairs derived from prior trajectories through the environment and use a Gaussian process classifier to generate the likelihood of an object at a query pose. We also introduce POM-Localization, which uses an observation model based on POMs to perform inference on a factor graph for globally consistent long-term localization. We present empirical results showing that POM-Localization is indeed effective at producing globally consistent localization estimates in challenging real-world environments and that POM-Localization improves trajectory estimates even when the POM is formed from partially incorrect data.

I. INTRODUCTION

Mobile robots deployed in real world environments with humans frequently encounter changes due to movable objects. Since localization algorithms that assume the world is static fare poorly in such dynamic environments, state-of-the-art long-term localization approaches explicitly model movable and moving objects in an attempt to improve robustness, but come with several limitations. Some of these approaches [1]–[5] attempt to discover which features persist over long time scales and either discard the remaining features or keep them only for short-term use. This reduces the information available for localization, particularly when such movable objects comprise a large portion of the scene, and can cause the localization estimate to drift over time. Other methods [6]–[8] impose assumptions about the configurations or movement patterns of objects that may not match the true dynamics of the environment.

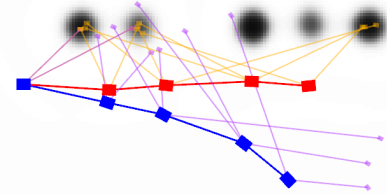
In many environments, movable objects tend to follow patterns, with some areas more likely to contain objects than others. Consider a parking lot like the one in Fig. 1a: the scene contains many movable objects, and consequently, this environment would challenge many localization algorithms.

The authors are with the Department of Computer Science, The University of Texas at Austin, Austin, TX. Email: {aaadkins, taijing, joydeepb}@cs.utexas.edu

This material is based upon work supported by the National Science Foundation (Graduate Research Fellowship Program under Grant No. DGE-2137420, CAREER-2046955), ARO (W911NF-19-2-0333), and Amazon. Any opinions, findings, and conclusions or recommendations expressed in this material are those of the author(s) and do not necessarily reflect the views of the National Science Foundation.



(a) Parking lot at three different times.



(b) POM for the above parking configuration, with more frequently occupied spots resulting in higher map values. An initial trajectory is shown in blue with object detections in purple. POM-Localization optimizes the trajectory (shown in red) so the corresponding object detections (shown in orange) is consistent with regions of high probability in the POM.

Fig. 1: POM-Localization as applied to a parking lot.

There is no fixed set of configurations and the individual objects may not have consistent periodic movement. However, such objects do follow a distribution that describes where they are likely to occur and where they are less likely. This holds true for other scenarios, such as pallets and boxes in warehouses or furniture in home and office environments.

We posit that localization algorithms can utilize the distribution of movable objects to improve robustness in real world environments. We introduce the concept of probabilistic object maps (POMs) to model the likelihood of a movable object of a given semantic class occurring at a given pose and propose a method for POM representation. The POM is formed in a data-driven manner from object detections from past trajectories and uses Gaussian process classification to generate likelihoods for new query poses. We also introduce the POM-Localization algorithm, which uses POMs to inform localization. The goal of POM-Localization is to prevent significant drift in environments with a high density of movable objects, rather than to improve average-case performance. Given the current estimate for the robot's trajectory and the object detections from that trajectory, POM-Localization calculates where objects would be in the global frame and adds a cost based on the likelihood of

an object occurring at the pose, penalizing the trajectory when objects would occur at unlikely poses. As shown in Fig. 1b, this formulation is used to optimize the trajectory, resulting in a sequence of poses that best aligns with current object detections, odometry measurements, and the POMs. We also provide a method for incrementally updating a POM given a newly optimized trajectory with object detections. We present experimental results on two different datasets to highlight the performance of POM-Localization in changing environments and to demonstrate the impact of our approach given limited knowledge of the object distribution represented in the POM.

II. RELATED WORK

A. Semantic SLAM and Localization

Similar to our method, semantic landmark SLAM and localization approaches rely on high-level semantic objects rather than low-level features. Many approaches, like [9], require data association by the feature extractor to associate measurements to landmarks. This can be challenging, particularly in dynamic environments, and mistakes can degrade results. Some methods try to improve robustness by shifting responsibility for data association to the optimization, allowing correspondence decisions to be updated as more information is obtained. Bowman et al. [10] propose a semantic SLAM approach that integrates data association into the optimization using expectation maximization, while [11] and [12] use factor graphs with novel factors that handle data association. Like these approaches, our method uses high-level semantic objects and does not require the feature extractor to resolve data associations. However, our approach avoids the correspondence problem altogether by considering a distribution of objects rather than a discrete set of landmarks. These approaches also differ from ours in that they do not explicitly model changes in environments.

B. Localization and Mapping in Changing Environments

While many SLAM and localization approaches assume objects in the scene are static, some methods explicitly model moving and movable objects. Some simply filter movable and/or moving objects from the data [1]. This improves robustness, but results in loss of information that could be valuable for localization. Others aim to understand which features persist over long time scales, with remaining features either discarded or kept only for short-term processing. [2] removes old data that conflict with more recent information. [3] probabilistically models feature persistence and [4] extends this approach to consider relationships between features. Episodic non-Markov Localization (EnML) [5] matches long-term features to a map and uses short-term features for relative corrections. Such methods require accurate data association to ensure the correct features are discarded and do not obtain global understanding from short-term features. In scenes with few long-term features, this can lead to drift in the localization estimate. Other approaches impose assumptions about the patterns of movable objects. Such assumptions include a limited range of possible configurations for regions

of the space [6] or that object movement conforms to some periodicity [7] or transition function [8]. For scenarios such as warehouses, parking lots, or areas with movable furniture, these assumptions may not appropriately model the real dynamics of the environment, and consequently, localization performance could degrade.

C. Continuous Mapping

Appropriate map representations are critical to localization and SLAM. Occupancy grids are commonly used, but introduce errors from discretization. The fixed resolution of occupancy grids is also poorly suited to variable density data and continuous optimization techniques used in many modern localization approaches. Recent works have explored continuous map representations to avoid these shortcomings. Hilbert maps [13] model the occupancy of an environment by projecting data into a Hilbert space, while [14] uses Bayesian Generalized kernel inference. In [15], occupancy is estimated with Gaussian process classification, similar to our approach to modeling object likelihood. These methods have been extended to handle dynamic environments in [16] and [17], but focus on observed motion, while the proposed method also accommodates objects that move between robot deployments. Further, all of these works focus on raw sensor data and do not incorporate semantics.

III. MAPPING AND LOCALIZATION WITH PROBABILISTIC OBJECT MAPS

We introduce the concept of probabilistic object maps (POMs), a POM representation based on Gaussian process classification (GPC), and the POM-Localization algorithm that uses POMs to inform robot localization in environments with movable objects. We also outline techniques to increase the speed of POM evaluation and POM-Localization. Our approach requires a set of initial trajectories with object detections from which to bootstrap the POMs for each environment. The POM-Localization algorithm also requires odometry estimates from either wheel encoders, inertial measurements, or visual odometry. To avoid assumptions about periodicity, our POM representation does not model temporal patterns.

A. POM Evaluation using Gaussian Process Classification

The goal of a POM is to estimate the likelihood that an object occurs at a given pose o^* . For this, we utilize a variant of GPC [18], chosen for its data-driven nature and continuous differentiability. Further, this data-driven method allows the POM to capture the distribution of errors arising from observation noise. The POM estimates the distribution $p(c^*=1|o^*)$, where $c^* \in \{0, 1\}$ is a class label indicating whether the pose is occupied by an object, with $p(c^*=1|o^*)$ evaluating to 1 when there should always be an object at pose o^* and 0 when there is never an object at the pose.

Let $o_{1:M}$ be the M sample inputs (object poses) for which we have corresponding output values (object occurrence likelihoods). GPC is closely related to Gaussian process regression (GPR), with the primary difference that the output

range of GPR is unbounded, while the output range of GPC is $[0, 1]$. Thus, GPC is a more appropriate function approximator for a classification distribution. GPC transforms the output $a^* \in (-\infty, \infty)$ of GPR using an activation function, such as the logistic function, $s(x) = \frac{1}{1+e^{-x}}$. For a 3D query pose o^* , this transformation via GPR and GPC is:

$$o^* \in \text{SE}(3) \xrightarrow{\text{GPR}} a \in (-\infty, \infty) \xrightarrow{s} t \in [0, 1] \quad (1)$$

$$\equiv o^* \in \text{SE}(3) \xrightarrow{\text{GPC}} t \in [0, 1]. \quad (2)$$

Traditionally, GPC assumes training output values $t_{1:M} \in \{0, 1\}$ and requires approximations to map these to $a_{1:M} \in (-\infty, \infty)$ as used by the underlying GPR model. We instead assume that we directly obtain sample values $a_{1:M}$ that are used with GPR and detail this process in Section III-C. The POM estimate $p(c^*=1|o^*)$ is thus given by GPC as

$$p(c^*=1|o^*) = \int p(c^*=1|a^*)p(a^*|a_{1:M}, o_{1:M}, o^*)da^*. \quad (3)$$

Based on GPR, $p(a^*|a_{1:M}, o_{1:M}, o^*)$ is a normal distribution having mean μ and variance σ^2 , with μ given by

$$\mu = \mu_0 + K_x^T K_D^{-1} (a - \mu_0), \quad (4)$$

where μ_0 is a prior mean in the range $(-\infty, \infty)$, $a - \mu_0$ is a vector of values $a_{1:M}$ less μ_0 ,

$$K_D = \begin{bmatrix} k(o_1, o_1) & \dots & k(o_1, o_M) \\ \vdots & k(o_i, o_j) & \vdots \\ k(o_M, o_1) & \dots & k(o_M, o_M) \end{bmatrix}, \quad (5)$$

$$K_x = \begin{bmatrix} k(o_1, o^*) \\ \vdots \\ k(o_M, o^*) \end{bmatrix}, \quad (6)$$

and $k(o_i, o_j)$ is a kernel function providing the similarity of o_i and o_j . The calculation of σ^2 is described in Section III-B.

$p(c^*=1|a^*)$ is the logistic function, making $p(c^*=1|o^*)$ the convolution of a normal distribution and the logistic function. We adapt the approximation from [18] for such a convolution to incorporate the prior mean μ_0 , giving

$$p(c^*=1|o^*) \approx s \left(\mu_0 + \frac{\mu - \mu_0}{\sqrt{1 + \frac{\pi\sigma^2}{8}}} \right). \quad (7)$$

For POM evaluation, the kernel for computing μ is a scaled product of a radial basis function (RBF) kernel [18] on position and a periodic variant of an RBF kernel on orientation. A prior for the likelihood of an object is transformed from $[0, 1]$ by the logit function to obtain μ_0 .

B. Uncertainty Estimation in POMs

Traditionally, GPR assumes that the output for a fixed input is drawn from a normal distribution and the output variance reflects the consistency of the samples near a given input. However, in our case, consistent values are not expected for each query input, so the traditional variance provided by GPR would yield high variance even where there are many samples and confidence in the distribution

should be high. Instead, predicting the likelihood of an object occurrence is closer to predicting coin bias, where we have a series of trials (past observations for poses) and we want to know the likelihood of an event (object occurrence at the given pose). Hence, we are computing σ^2 using an approach derived from the desired properties of the variance: more sample inputs should result in lower variance and samples that are closer to the query pose o^* should result in lower variance than the same number of more distant samples. Consequently, we estimate σ^2 using the reciprocal of an unnormalized kernel density estimator (KDE) [18], which satisfies these conditions. Using this, σ^2 is given by

$$\sigma^2(o^*) = \frac{1}{\text{KDE}(o^*)} = \frac{1}{\sum_{i=1}^M k_\sigma(o_i, o^*)}, \quad (8)$$

where k_σ has the same form as the kernel for computing μ .

C. Building Probabilistic Object Maps

To evaluate the likelihood of an object occurring at a given pose using GPC, we need a set of samples $\langle o_i, a_i \rangle_{i=1:M}$, where o_i is a pose in the global frame and $a_i \in (-\infty, \infty)$ represents the object likelihood at the pose based on past trajectories. When the POM is initially created, we use a set of registered trajectories and their object detections. To capture where objects are both likely and unlikely, we obtain $\{o_i\}$ from 1) observed object poses from the registered trajectories as well as 2) poses where objects were not observed, generated by sampling from the observed free space around the robot. The next step is generating values a_i for each sample pose o_i . Given a set of object detection poses $S_t = \{s_{t_j}\}$ relative to the robot at time t_j and corresponding variances $\{\sigma_{t_j}^2\}$, the value \hat{a}_i for a sample pose \hat{o}_i relative to the robot can be obtained using

$$\hat{a}_i = \max_{s_{t_j} \in S_t} \mathcal{N}(\hat{o}_i | s_{t_j}, \sigma_{t_j}^2). \quad (9)$$

If there are no object detections, then \hat{a}_i is 0. We remap each \hat{a}_i from $[0, \infty)$ to $a_i \in (-\infty, \infty)$ using a domain remapping to match the expected input range of the logistic function.¹ In our approach, a separate POM is created for each movable object class (e.g. separate POMs for cars vs. bicycles).

D. POM-Localization

POM-Localization incorporates odometry and object detections to estimate the belief over the robot's trajectory. The POM value for observed object poses is used to calculate the observation likelihood. We introduce a POM observation likelihood (POM-OL) that is general to several forms of semantic object detections, such as those provided by object pose detectors [19] and semantic segmentation [20]. POM-OL requires the ability to draw object pose samples $\hat{o}_{i_k} \sim p(\hat{o}_{i_k} | r_{i_k})$, where r_{i_k} is relative object detection information. We first present the POM-Localization algorithm, followed by two such formulations of the POM-OL in Section III-E.

¹The choice of the remapping function is not crucial, as long as it is a monotonic injective mapping. We use $a_i = \log(1 - (1 - \exp(\hat{a}_i))^{-1})$.

The belief over the robot poses $x_{1:n}$ is given by

$$\text{Bel}(x_{1:n}) = p(x_{1:n}|x_0, s_{1:n}, u_{1:n}) \quad (10)$$

$$\propto \prod_{i=1}^n \prod_{k=1}^{N_i} p(s_{i_k}|x_i) \prod_{j=0}^{n-1} p(x_{j+1}|x_j, u_{j+1}), \quad (11)$$

where N_i is the number of detections of objects at pose x_i , s_{i_k} is the k th object detection ($k \in [1, N_i]$) relative to the robot at pose x_i , and u_i is the odometry measurement from x_{i-1} to x_i with covariance Σ_{odom} . s_{i_k} is composed of information about the object's pose r_{i_k} and classification variable c_{i_k} , and, as we do not consider negative information about objects, $c_{i_k}=1$ for all s_{i_k} . Next, the observation likelihood $p(s_{i_k}|x_i) = p(r_{i_k}, c_{i_k}=1|x_i)$ can be written as

$$p(s_{i_k}|x_i) = p(r_{i_k}|x_i, c_{i_k}=1)p(c_{i_k}=1|x_i). \quad (12)$$

To use the object likelihood in the belief, we marginalize over the true object pose o_{i_k} in the global frame. We can express $p(r_{i_k}|x_i, c_{i_k}=1)$ in terms of o_{i_k} as

$$p(r_{i_k}|x_i, c_{i_k}=1) = \int_{o_{i_k}} p(r_{i_k}|o_{i_k}, x_i) p(o_{i_k}|x_i, c_{i_k}=1) do_{i_k} \quad (13)$$

$$= \int_{o_{i_k}} p(r_{i_k}|o_{i_k}, x_i) p(c_{i_k}=1|x_i, o_{i_k}) \frac{p(o_{i_k}|x_i)}{p(c_{i_k}=1|x_i)} do_{i_k}. \quad (14)$$

Since the existence of an object is independent of the robot's pose, i.e. $p(o_{i_k}|x_i) = p(o_{i_k})$, combining (12) and (14) yields

$$p(s_{i_k}|x_i) = \int_{o_{i_k}} p(r_{i_k}|o_{i_k}, x_i) p(c_{i_k}=1|o_{i_k}) p(o_{i_k}) do_{i_k}. \quad (15)$$

Substituting (15) into (11) gives an updated form for the belief. We solve for the maximum likelihood estimate $x_{1:n}^*$ by minimizing the negative log likelihood of the belief:

$$\begin{aligned} -\log(\text{Bel}(x_{1:n})) &\propto \frac{1}{2} \sum_{j=0}^{n-1} \|x_{j+1} \ominus (x_j \oplus u_{j+1})\|_{\Sigma_{\text{odom}}}^2 + \\ &\sum_{i=1}^n \sum_{k=1}^{N_i} -\log \int_{o_{i_k}} p(r_{i_k}|o_{i_k}, x_i) p(c_{i_k}=1|o_{i_k}) p(o_{i_k}) do_{i_k}. \end{aligned} \quad (16)$$

The integral above is intractable, so we approximate it by sampling. Noting that the relative pose detection r_{i_k} is independent of x_i conditioned on the relative object pose $\hat{o}_{i_k} = o_{i_k} \ominus x_i$, and applying Bayes' rule, we replace $p(r_{i_k}|o_{i_k}, x_i)$ with $p(\hat{o}_{i_k}|r_{i_k})$ to yield

$$\begin{aligned} \int_{o_{i_k}} p(r_{i_k}|o_{i_k}, x_i) p(c_{i_k}=1|o_{i_k}) p(o_{i_k}) do_{i_k} &\propto \\ &\int_{o_{i_k}} p(\hat{o}_{i_k}|r_{i_k}) p(c_{i_k}=1|o_{i_k}) p(o_{i_k}) do_{i_k}. \end{aligned} \quad (17)$$

As noted above, we assume that our observation model supports drawing samples from $p(\hat{o}_{i_k}|r_{i_k})$. We can thus approximate the integral using importance sampling by drawing N_s samples $\hat{o}_{i_k s}$ from $p(\hat{o}_{i_k s}|r_{i_k})$, obtaining the corresponding

global frame pose $o_{i_k s}$ from the sample using $o_{i_k s} = x_i \oplus \hat{o}_{i_k s}$, and then summing. With normalization constant η_1 , this gives

$$\begin{aligned} \int_{o_{i_k}} p(r_{i_k}|o_{i_k}, x_i) p(c_{i_k}=1|o_{i_k}) p(o_{i_k}) do_{i_k} &\approx \\ \frac{\eta_1}{N_s} \sum_{s=1}^{N_s} p(c_{i_k s}=1|o_{i_k s}) p(o_{i_k s}). \end{aligned} \quad (18)$$

We assume $p(o_{i_k})$ is uniform, so we can replace this by a normalization constant $\frac{\eta_2}{N_s}$, yielding

$$\frac{1}{N_s} \sum_{s=1}^{N_s} p(c_{i_k s}=1|o_{i_k s}) p(o_{i_k s}) \approx \frac{\eta_2}{N_s} \sum_{s=1}^{N_s} p(c_{i_k s}=1|o_{i_k s}). \quad (19)$$

Since the normalization constant is independent of the trajectory, we drop η_2 . Combining (16), (18) and (19) gives

$$\begin{aligned} -\log(\text{Bel}(x_{1:n})) &\propto \frac{1}{2} \sum_{j=0}^{n-1} \|x_{j+1} \ominus (x_j \oplus u_{j+1})\|_{\Sigma_{\text{odom}}}^2 + \\ &\sum_{i=1}^n \sum_{k=1}^{N_i} -\log \left(\frac{1}{N_s} \sum_{s=1}^{N_s} p(c_{i_k s}=1|o_{i_k s}) \right). \end{aligned} \quad (20)$$

With this formulation and the POM to provide object likelihoods $p(c_{i_k s}=1|o_{i_k s})$, a nonlinear optimizer, such as [21], can be used to find the trajectory $x_{1:n}$ that best aligns with the movable object observations and odometry.

E. Observation Models

The first observation model uses a relative pose measurement of the object for each observation r_{i_k} . For this model, we assume $p(r_{i_k}|\hat{o}_{i_k})$ is a normal distribution. Since this is symmetric with respect to r_{i_k} and \hat{o}_{i_k} , we can thus sample object poses via the normal distribution. The second observation model uses semantically-labeled points relative to the robot's sensor for each observation r_{i_k} . In this model, we approximate $p(\hat{o}_{i_k}|r_{i_k})$ as a histogram over the space of object poses. The value for each bin in the histogram is computed using a method based on the generalized Hough transform [22], enabling generated samples to be robust to partial observations. We assume a fixed shape and size for each class of object. Sensor noise is accounted for by adding Gaussian noise to each observed point. Given the observed points, we sample points along the object's surface where each of the observed points could occur. From these sampled points, we compute the object's pose in the sensor frame and add a vote for the corresponding bin. To discard outliers, bins with values less than a specified threshold are discarded. The remaining candidate poses are randomly sampled to generate object pose samples to evaluate with the POM.

F. Updating the POM Based on New Trajectories

We can update the POM to incorporate information from a newly optimized trajectory to better capture the true distribution of objects in the environment. We generate new sample poses and values using the same process outlined in Section III-C with the sampled object poses based on object observations $\{s_{i_k}\}$, robot fields of view, and optimized poses

$x_{1:n}$ from the new trajectory. These new samples are added to the existing samples to form the updated POM, which can be used to optimize subsequent trajectories.

G. Optimization for Computational Efficiency

As Gaussian processes are computationally expensive, we employ a number of mechanisms to make the speed of this approach tractable. The first is limiting the samples used to compute μ and σ^2 in the POM evaluation to those within a radius of the query pose. We do this by storing the sample poses and values in a KD-tree [23] and constructing a POM at the beginning of each optimization cycle with only samples around the initial estimate for the object pose. Using a subset of the sample poses and outputs when evaluating the POM also reduces the computation time. Let r_s be the fraction of the samples to use and M be the full number of samples. We adjust the POM evaluation by modifying (8) to sum instead over $N = r_s M$ random samples and compensate for subsampling by multiplying the full equation by r_s . We can also scale the computational power needed by modifying the number of samples N_s used to approximate the marginalization over object poses. Lastly, using only a subset of the object detections and optimizing over a window of only the most recent nodes in the trajectory improves computation time.

IV. EXPERIMENTAL RESULTS

We present results from two sets of experiments² that evaluate POM-Localization’s ability to 1) accurately estimate trajectories when knowledge of the distribution of movable objects is limited and the correctness of the POM is varied, and 2) ensure consistency in global localization over long time scales in environments with movable objects. We also provide qualitative results for a trajectory in a parking lot using semantically-labeled points. In these experiments, we focus on lidar-based approaches, as the increased field of view and sensor range associated with lidar are important for localization in changing environments.

A. Observation Models

These experiments use the two observation models described above. For results using the Hough transform-based model, we approximate cars as 2D rectangles the size of a Toyota Camry. We generate votes for object poses from line segments connecting neighboring points by choosing a random location on the rectangle where the line segment would fall. Examples of observed points and corresponding generated samples are shown in Fig. 2.

B. Accuracy Given Limited Object Distribution Knowledge

We aim to understand how quality of data used to form the POM impacts trajectory estimates when we have not captured the full distribution of objects and we assume low confidence in our map, which would occur when we have not

²The code for POM-Localization and our experiments is available at https://github.com/ut-amrl/pom_localization and uses [21] for optimization.

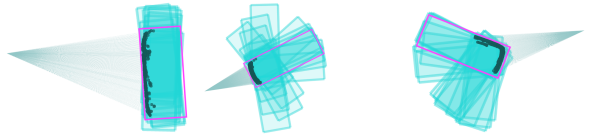


Fig. 2: Examples of observed point clusters and generated object pose samples. True object poses are shown in pink.

collected sufficient past trajectories to converge to the true distribution. To do so, we measure accuracy using absolute trajectory error (ATE) on 10 sequences from the KITTI dataset [24] and compare against the output of LeGO-LOAM [25], a state-of-the-art lidar-inertial odometry and mapping algorithm. Though our method supports 3D, we use a 2D projection for these experiments to match the 2D projection used for object observations. The trajectory estimates of LeGO-LOAM serve as our odometry constraints. We demonstrate our approach using both semantically-labeled points and object poses. In both cases, data is derived from “car” instances in the SemanticKITTI dataset [26], which contains labels for lidar scan points in the KITTI benchmark (sequence 01 was excluded due to lack of “car” observations). The labeled points come directly from the dataset and object detections are created by transforming the global pose of each object into the frame in which the instance was observed.

To assess the impact of the correctness of the POM, we test five different configurations. In all cases, we generate the POM from a single simulated past trajectory, and thus have low confidence in our distribution to emulate the range of performance when bootstrapping the POM from one or few observed past trajectories. The initial step in creating the POM is generating poses where cars occurred in the past trajectory: $X\%$ of simulated car poses for the first four configurations are obtained by selecting poses from the current trajectory’s observed cars and adding a small amount of Gaussian noise (0.4 m), with the remaining $Y\%$ randomly placed in the environment. As X increases, the correctness of the POM increases. We chose X from $\{0, 20, 50, 80, 100\}$ in our experiments, and these are denoted “POM-Localization (X - Y)” in Table I. In the last configuration, POM-Localization (100 $^+$ -0), the POM is created from the same car poses that were used to generate the detections without any added noise, simulating perfect knowledge of the distribution and a deterministic environment in which movable objects are always at the same poses. In all cases, once the simulated car poses are selected, we generate the POM following the steps in section III-C, with the ground truth trajectory as the prior trajectory, the relative poses of nearby simulated cars with added noise as past object detections, and a fixed-radius region around the trajectory poses as the free space for obtaining off-detection samples.

Table I shows the ATE for LeGO-LOAM and our approach with the five configurations using object detections and semantic segmentation. When the POMs are completely misaligned with the observations as in POM-Localization (0-

	KITTI Sequence Number	00	02	03	04	05	06	07	08	09	10
Object Detections	LeGO-LOAM	27.12	1630.55	3.51	4.11	7.97	1.19	0.76	113.44	6.48	1.76
	POM-Localization (0-100)	29.46	1630.55	3.51	4.11	7.97	0.80	0.76	113.44	6.48	1.76
	POM-Localization (20-80)	22.93	1630.55	3.55	4.11	1.83	0.37	0.20	113.44	6.48	1.76
	POM-Localization (50-50)	1.73	1322.19	1.39	4.06	1.95	0.08	0.03	106.86	0.80	0.33
	POM-Localization (80-20)	1.50	1332.74	0.89	4.10	1.71	0.09	0.04	113.42	0.81	1.06
	POM-Localization (100 ⁺ -0)	1.59	1333.48	0.82	4.04	0.18	0.04	0.04	97.58	0.23	0.17
Semantic Segmentation	POM-Localization (0-100)	37.37	1553.24	3.52	4.11	5.43	1.63	0.79	111.50	9.78	3.23
	POM-Localization (20-80)	6.30	1570.66	3.22	4.09	1.14	0.28	0.22	97.24	1.08	1.97
	POM-Localization (50-50)	0.37	1203.31	2.00	4.06	2.27	0.24	0.06	91.43	0.80	0.96
	POM-Localization (80-20)	0.31	1408.15	0.88	4.09	1.60	0.17	0.07	69.33	0.60	0.79
	POM-Localization (100 ⁺ -0)	0.28	1417.72	0.85	4.06	1.30	0.15	0.05	36.51	0.45	0.60

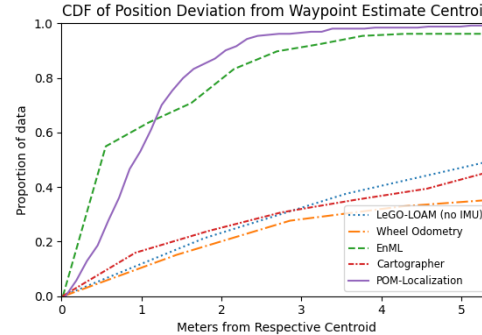
TABLE I: Absolute Trajectory Error (m) on KITTI dataset sequences for LeGO-LOAM and POM-Localization using observation models for object detections and semantic segmentation.

100), estimates are comparable to the LeGO-LOAM results. For the results using object detections, estimates for all but one sequence have the same or lower error and the remaining estimate having only 8.6% higher ATE than the LeGO-LOAM result. For the semantic segmentation results, estimates for four sequences have somewhat worse error for the completely misaligned POM configuration. However, it is unlikely in practice that all observations in a given trajectory will be completely disjoint from past data. This can also be mitigated by placing higher weight on odometry; however, we aimed to balance the worst-case and best-case performances. As POM correctness increases, results generally improve, with the ATE of most trajectories generated using the POM created from perfect knowledge substantially lower than the ATE for LeGO-LOAM estimates. In most cases, even a half-correct map substantially improves the trajectory estimates. The only sequences for which our approach does not substantially improve upon LeGO-LOAM are 02, 04 and 08. In all of these sequences, there were trajectory segments that simultaneously had substantial odometry error and few or no object detections, and, as odometry is weighted highly relative to object detections, the drift was not corrected and persisted for the remainder of the trajectories.

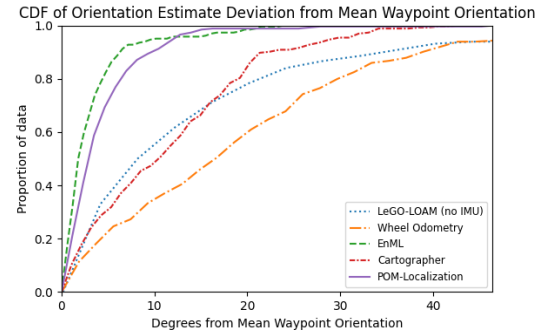
C. Consistency Over Trajectories in Changing Environments

To understand our approach’s ability to produce consistent localization estimates over long time scales in changing environments, we collected eight trajectories over four days in a UT Austin campus parking lot using a Clearpath Jackal with a Velodyne VLP-16 Lidar. In each trajectory, the robot started and ended at the same location and visited 32 waypoints consistent across all trajectories, while the segments between the waypoints varied. The trajectories had an average length of 372 meters and an average duration of 26 minutes. The percent of mapped parking spots occupied by cars ranged from 11% to 92%, with an average of 60%.

Data used for these experiments were collected in 2D. Odometry constraints are obtained from wheel odometry and object detections are derived from human-provided annotations of point clouds. The POM is generated from a manually-created map of parking spots to demonstrate resilience to deviations from the true car distribution and to eliminate the quality of the localization algorithm used to



(a) CDF of position estimate deviation.



(b) CDF of orientation estimate deviation.

Fig. 3: Position and orientation consistency across approaches. An optimal algorithm would quickly rise to 1.

bootstrap the POM as a variable in the results. We simulate five possible parking configurations by randomly selecting 70% of the parking spots to be occupied and placing cars according to a normal distribution around each selected spot. Samples to form the POM are created by simulating trajectories through each of the parking configurations, transforming the object poses to the frame of each node, and adding Gaussian noise to simulate noisy detection in past trajectories. Off-detection sample poses are drawn from within a radius around nodes in each simulated trajectory.

We assess performance by measuring consistency of waypoint estimates over the eight trajectories. Position estimate consistency is evaluated by calculating the centroid of all estimates for each waypoint across all trajectories and finding

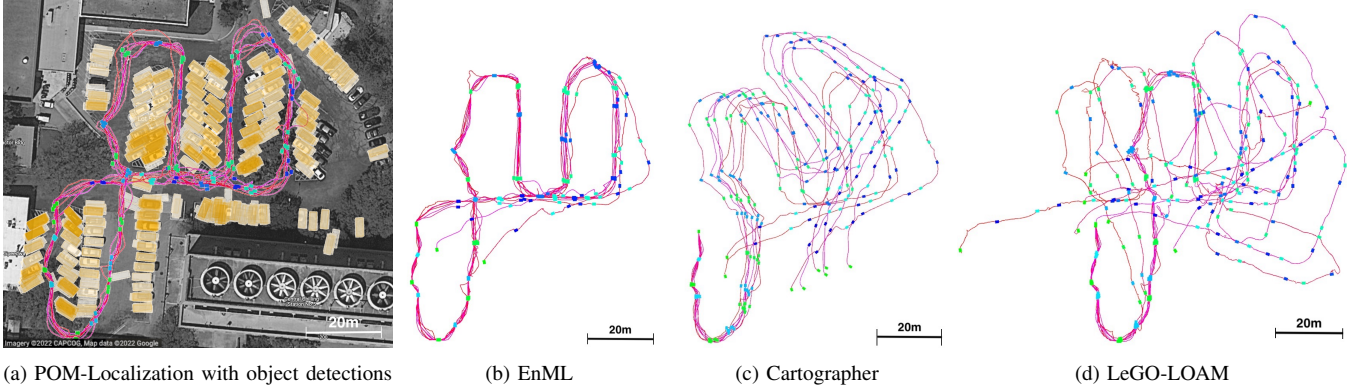


Fig. 4: Plots of trajectories through UT Austin Lot 53 as estimated by the approaches with highlighted blue/green waypoints. Performance of an approach is good when all estimates for a given waypoint are colocated. POM-Localization results are overlayed on a satellite view and shown with aggregated object poses from all trajectories.

the distance of each estimate from the centroid. Similarly, the orientation consistency is measured by computing the mean orientation estimate for each waypoint and the distance of each estimate from the corresponding mean orientation. We show the results of POM-Localization compared to estimates from wheel odometry, Cartographer [27] (a commonly used mapping and localization package), LeGO-LOAM [25] without use of an inertial measurement unit (IMU), and EnML [5]. Cartographer built a map during a single run and used this map in localization mode for the remainder of the trajectories, while EnML matches long-term features to a manually-created map and uses short-term features for local matching. It should be noted that the map and point clouds used by EnML are higher fidelity than the object detections and POM used by POM-Localization.

Fig. 3 shows the cumulative distribution functions (CDFs) for the position and orientation estimate consistency. For both position and orientation, POM-Localization significantly outperforms raw wheel odometry, Cartographer, and LeGO-LOAM. EnML has slightly better average-case performance; this is expected, as the higher-fidelity data used by EnML enables a higher-precision result. However, POM-Localization has better or comparable worst-case performance: a greater portion of the orientation estimates are within 15 degrees of the mean for POM-Localization as compared to EnML and no position estimate from POM-Localization deviates more than 5.5 meters from its waypoint centroid. The trajectories and waypoints estimated by POM-Localization, EnML, Cartographer, and LeGO-LOAM are shown in Fig. 4. These plots support the conclusions drawn from Fig. 3; the estimates from LeGO-LOAM and Cartographer drift substantially after the initial segment of the trajectory, while POM-Localization results in slightly greater spread for the waypoint estimates than EnML, but unlike EnML, has no trajectory estimates that diverge significantly. Fig. 4a also shows that the object pose estimates align with the true parking spots and with each other over time.

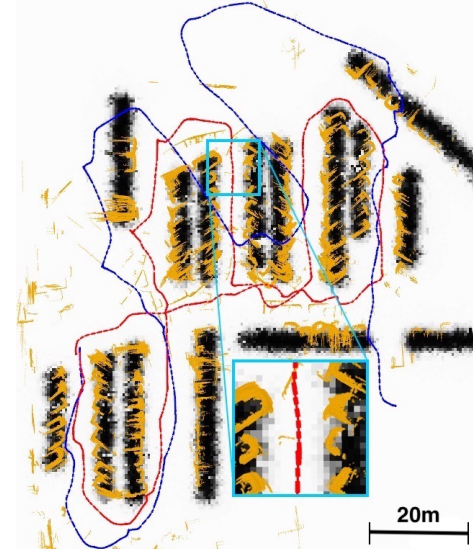


Fig. 5: POM-Localization optimized trajectory (red) vs. odometry estimate (blue), with semantic point observations in orange, and POM in greyscale. Inlay shows alignment of semantic point observations of cars and the alignment with the POM.

D. Parking Lot Localization With Labeled Points

Fig. 5 shows a trajectory before and after optimization using POM-Localization with semantically-labeled lidar points for car clusters. The trajectory from odometry is shown in blue and the optimized trajectory is shown in red. Object observations for cars are semantically-labeled clusters of points from a 3D point cloud obtained using a heuristic-based segmentation algorithm, which can be found in our repository.² This algorithm uses PCL [28] for clustering and returns clusters that match expected properties of cars. The background of the figure shows a discretized version of the POM, with areas likely to have cars in black and those unlikely to have cars in white. The semantically-labeled points, transformed using the robot pose estimates, are shown in orange. The car segmentation algorithm gives several false positive detections resulting from other objects in the environment and cars in motion are also observed. Despite

this, POM-Localization is able to optimize the trajectory so that the stationary cars line up with peaks in the POM. There is some variation in the resulting pose of each car. However, this is to be expected: the POM is not sharply peaked, so that it can accommodate variations in parked car poses over time, and POM-Localization works without performing data association between sensor data across timesteps. The optimized trajectory begins and ends at approximately the same pose, showing that POM-Localization successfully corrected drift from odometry.

V. CONCLUSION AND FUTURE WORK

This paper presents probabilistic object maps to model the distribution of movable objects in an environment. We also introduce POM-Localization to incorporate object detections and corresponding POMs to achieve globally consistent localization in changing environments, thus enhancing the ability of robots to perform autonomously.

There are a number of interesting areas for future exploration. Though our enhancements improved speed, investigation of other approximations may further reduce computation time. Future improvements could also include modifying our model to work with monocular visual detectors. Additionally, the POM-Localization observation factors could be integrated into an approach with other factors, such as short-term features or loop closures, allowing the combined approach to gain the benefits of all such factors. We would also like to explore use of the Generalized Hough transform [22] with a more complex shape model or learned method similar to VoteNet [29] to propose occlusion-tolerant object pose samples for more complex models. If the object periodicity is known, time could be incorporated into the GPC kernel to model temporal patterns. Finally, POMs could be applied to other problems such as navigation to avoid likely occupied areas or finding objects in home environments.

REFERENCES

- [1] S. Zhao, Z. Fang, H. Li, and S. Scherer, “A robust laser-inertial odometry and mapping method for large-scale highway environments,” in *2019 IEEE/RSJ International Conference on Intelligent Robots and Systems (IROS)*. IEEE, 2019, pp. 1285–1292.
- [2] A. Walcott-Bryant, M. Kaess, H. Johannsson, and J. J. Leonard, “Dynamic pose graph SLAM: Long-term mapping in low dynamic environments,” in *2012 IEEE/RSJ International Conference on Intelligent Robots and Systems*. IEEE, 2012, pp. 1871–1878.
- [3] D. M. Rosen, J. Mason, and J. J. Leonard, “Towards lifelong feature-based mapping in semi-static environments,” in *2016 IEEE International Conference on Robotics and Automation (ICRA)*. IEEE, 2016, pp. 1063–1070.
- [4] F. Nobre, C. Heckman, P. Ozog, R. W. Wolcott, and J. M. Walls, “Online probabilistic change detection in feature-based maps,” in *2018 IEEE International Conference on Robotics and Automation (ICRA)*. IEEE, 2018, pp. 3661–3668.
- [5] J. Biswas and M. M. Veloso, “Episodic non-markov localization,” *Robotics and Autonomous Systems*, vol. 87, pp. 162–176, 2017.
- [6] C. Stachniss and W. Burgard, “Mobile robot mapping and localization in non-static environments,” in *AAAI*, 2005, pp. 1324–1329.
- [7] T. Krajník, J. P. Fentanes, J. M. Santos, and T. Duckett, “FrEMEn: Frequency map enhancement for long-term mobile robot autonomy in changing environments,” *IEEE Transactions on Robotics*, vol. 33, no. 4, pp. 964–977, 2017.
- [8] G. D. Tipaldi, D. Meyer-Delius, and W. Burgard, “Lifelong localization in changing environments,” *The International Journal of Robotics Research*, vol. 32, no. 14, pp. 1662–1678, 2013.
- [9] S. Yang and S. Scherer, “CubeSLAM: Monocular 3-D object SLAM,” *IEEE Transactions on Robotics*, vol. 35, no. 4, pp. 925–938, 2019.
- [10] S. L. Bowman, N. Atanasov, K. Daniilidis, and G. J. Pappas, “Probabilistic data association for semantic SLAM,” in *2017 IEEE International Conference on Robotics and Automation (ICRA)*. IEEE, 2017, pp. 1722–1729.
- [11] K. Doherty, D. Fourie, and J. Leonard, “Multimodal semantic SLAM with probabilistic data association,” in *2019 International Conference on Robotics and Automation (ICRA)*. IEEE, 2019, pp. 2419–2425.
- [12] K. J. Doherty, D. P. Baxter, E. Schneeweiss, and J. J. Leonard, “Probabilistic data association via mixture models for robust semantic SLAM,” in *2020 IEEE International Conference on Robotics and Automation (ICRA)*. IEEE, 2020, pp. 1098–1104.
- [13] F. Ramos and L. Ott, “Hilbert maps: Scalable continuous occupancy mapping with stochastic gradient descent,” *The International Journal of Robotics Research*, vol. 35, no. 14, pp. 1717–1730, 2016.
- [14] K. Doherty, T. Shan, J. Wang, and B. Englot, “Learning-aided 3-D occupancy mapping with Bayesian generalized kernel inference,” *IEEE Transactions on Robotics*, vol. 35, no. 4, pp. 953–966, 2019.
- [15] S. T. O’Callaghan and F. T. Ramos, “Gaussian process occupancy maps,” *The International Journal of Robotics Research*, vol. 31, no. 1, pp. 42–62, 2012.
- [16] R. Senanayake, L. Ott, S. O’Callaghan, and F. Ramos, “Spatiotemporal Hilbert maps for continuous occupancy representation in dynamic environments,” in *Proceedings of the 30th International Conference on Neural Information Processing Systems*, 2016, pp. 3925–3933.
- [17] S. T. O’Callaghan and F. T. Ramos, “Gaussian process occupancy maps for dynamic environments,” in *Experimental Robotics*. Springer, 2016, pp. 791–805.
- [18] C. Bishop, *Pattern Recognition and Machine Learning*. Springer, January 2006. [Online]. Available: <https://www.microsoft.com/en-us/research/publication/pattern-recognition-machine-learning/>
- [19] E. Arnold, O. Y. Al-Jarrah, M. Dianati, S. Fallah, D. Oxtoby, and A. Mouzakitis, “A survey on 3D object detection methods for autonomous driving applications,” *IEEE Transactions on Intelligent Transportation Systems*, vol. 20, no. 10, pp. 3782–3795, 2019.
- [20] J. Zhang, X. Zhao, Z. Chen, and Z. Lu, “A review of deep learning-based semantic segmentation for point cloud,” *IEEE Access*, vol. 7, pp. 179 118–179 133, 2019.
- [21] S. Agarwal, K. Mierle, and T. C. S. Team, “Ceres Solver,” 3 2022. [Online]. Available: <https://github.com/ceres-solver/ceres-solver>
- [22] D. H. Ballard, “Generalizing the hough transform to detect arbitrary shapes,” *Pattern recognition*, vol. 13, no. 2, pp. 111–122, 1981.
- [23] J. L. Bentley, “Multidimensional binary search trees used for associative searching,” *Communications of the ACM*, vol. 18, no. 9, pp. 509–517, 1975.
- [24] A. Geiger, P. Lenz, and R. Urtasun, “Are we ready for autonomous driving? The KITTI vision benchmark suite,” in *2012 IEEE Conference on Computer Vision and Pattern Recognition*. IEEE, 2012, pp. 3354–3361.
- [25] T. Shan and B. Englot, “LeGO-LOAM: Lightweight and ground-optimized lidar odometry and mapping on variable terrain,” in *2018 IEEE/RSJ International Conference on Intelligent Robots and Systems (IROS)*. IEEE, 2018, pp. 4758–4765.
- [26] J. Behley, M. Garbade, A. Milioto, J. Quenzel, S. Behnke, C. Stachniss, and J. Gall, “SemanticKITTI: A dataset for semantic scene understanding of LiDAR sequences,” in *2019 IEEE/CVF International Conference on Computer Vision (ICCV)*. IEEE, 2019, pp. 9296–9306.
- [27] W. Hess, D. Kohler, H. Rapp, and D. Andor, “Real-time loop closure in 2D LiDAR SLAM,” in *2016 IEEE International Conference on Robotics and Automation (ICRA)*, 2016, pp. 1271–1278.
- [28] R. B. Rusu and S. Cousins, “3D is here: Point Cloud Library (PCL),” in *IEEE International Conference on Robotics and Automation (ICRA)*. Shanghai, China: IEEE, May 9-13 2011.
- [29] C. R. Qi, O. Litany, K. He, and L. J. Guibas, “Deep hough voting for 3d object detection in point clouds,” in *Proceedings of the IEEE International Conference on Computer Vision*, 2019.